RESEARCH ARTICLE | MAY 22 2023

Investigation of soft robotic hand using tendon-driven mechanism of robotic manipulator

Danu Jaya Saputro ✉; Erfu Yang

AIP Conf. Proc. 2580, 040011 (2023)
https://doi.org/10.1063/5.0123384

Investigation of Soft Robotic Hand Using Tendon-Driven Mechanism of Robotic Manipulator

Danu Jaya Saputro [a)] and Erfu Yang [b)]

Department of Design, Manufacturing and Engineering Management
University of Strathclyde, Glasgow G1 1XJ, United Kingdom

[a)] Corresponding author: danu.saputro.2020@uni.strath.ac.uk
[b)] erfu.yang@strath.ac.uk

Abstract. A soft robotic hand is a robotic end-effector that can pick and place objects with high flexibility to handle fragile objects and adapt to unstructured and irregular shapes. One promising approach to handling soft objects is combining the rigid structure of the tendon-driven robot hand with elastomeric or rubber elements. It is essential to elaborate the tendon-driven mechanisms either in the closed-loop or open-loop kinematic system o obtain proper behavior of the under-actuation robotic hand. More specifically, the functional representation of kinematic construction of related components like shafts, pulley, and tendons must be carefully considered. This paper presents a systematic review of some recent technological advances in the area of soft robotic grippers. To analyze the tendon-driven mechanism (TDM), the kinematic synthesis is performed in this paper using graph theory. After the displacement equations are generated, the input and output torque (forces) connections are further appropriately obtained. Finally, a proposed design is given for a soft 2 degree of freedom (DOF) robotic gripper through exploring the openhand Yale model T, which employs soft rubber as the connector to each rigid link.

INTRODUCTION

As one development of robotic grippers/end-effectors, a soft robotic hand can pick and place objects with high flexibility when grasping and manipulating delicate objects and adjusting to unstructured and asymmetric shapes [1]. In addition to that, some soft robotics arms with a soft gripper made from silicone rubber material can move a part of the body dexterously by mimicking natural ability, such as extending, expanding, twisting, and bending towards the destination [2]. Another interesting point is that most soft grippers can grab and hold relatively soft objects, such as strawberries, chilly, tomatoes, etc.

The existing soft robotics solutions are widely varied according to the underlying technologies and materials. Shintake et al. [3] categorized soft gripper technologies in three different groups: i)actuator configuration, ii) controlled stiffness mechanism, and iii) adhesive technology. However, even though tremendous progress has emerged, an unstable system has remained a limitation. For example, the fluidic elastomer actuator (FEAs) is well known as the most mature soft robotic technology. Yet, the external pumps and fluid compressor may sometimes face obstacles in driving the actuator. Granular jamming and dry adhesion work properly in a vacuum but have challenges when handling rough surfaces and manipulating soft and deformable objects [3].

One promising approach to handling soft objects is combining the rigid structure of tendon-driven robot hand with elastomeric rubber material. In [4], it was conducted to replace the articulated segments and joints of the gripper with elastomers. Using adaptive hands with tendon-driven system, the structural compliance was embedded in the joints or finger-pads to increase the mechanical capability in conforming and grasping mechanism [5].

The limitation that the tendon-driven soft grippers could experience is the hindrance to designing smaller components of the entire configuration, including the usage of external motors [3]. This tendon-driven mechanism (TDM) also links closely with the under-actuated hand (fewer motors control the multi degree of freedoms), in which Bicchi et al. [6] argued that designing the robotic hands with a limited number of actuators could emerge the

Engineering Physics International Conference 2021 – EPIC 2021
AIP Conf. Proc. 2580, 040011-1–040011-10; https://doi.org/10.1063/5.0123384
Published by AIP Publishing. 978-0-7354-4484-3/$30.00

challenges for roboticists. For the ideal behavior of the under-actuation robotic hand, it is essential to elaborate on the tendon-driven mechanisms either in the closed-loop or open-loop kinematic configuration. More specifically, the functional representation of kinematic components, including shafts, pulley, and tendons, needs to be considered. [7]

This paper investigates the kinematic synthesis of tendon-driven robotic configuration based on Yale open hand model T using the graph theory. The graph representation related to the kinematic construction and the working principle is initially set up to generate the velocity and static moment equations [7].

PROBLEM OVERVIEW

Many kinematic structures of an articulated robot often employ an open-loop kinematic chain configuration. The reason behind this is the simplicity and easiness of construction. Unfortunately, to reach the desired state, the actuators are supposed to be located in the joint axes, increasing the robot's inertia load. To address this issue, a Three Degree of Freedom (DoF) robot, Cincinnati Milacron T^3, with a partial closed-loop kinematic chain structure, has been customized to be capable of reducing the inertia load. This robot mechanism utilized a bevel-gear train to attach the actuators remotely from the wrist structure.

Some advantages in the tendon-driven or belts mechanism are due to the inertia reduction in force transmission field and the remote-control ability [8-13]. In demonstrating the kinematic structure of the tendon-driven robot, Tsai [8] figured out the similarity to the epicycle gear train's mechanism. The kinematic analysis can be elaborated using the graph theory. After the displacement equations are generated, the input and output torque (forces) connections can be further appropriately obtained.

In order to successfully utilize belts or pulleys in a tendon-driven mechanism (TDM), gear trains are the important part to consider. They are employed to distribute power or movement related to parallel or nonparallel shafts, especially within small offsets. However, in a particular situation, intermediate shafts and idle gears are sometimes needed to respond if the corresponding two offset shafts create a larger center distance.

Despite the merits, as mentioned earlier, tendon transmission has limitations in some particular areas. Although the mechanical compliance offered by tendon-driven robotic hands is better than the motor-driven robotic ones, it requires a far more complex control system due to the tendon flexibility. Even more, it hinders the accuracy in positioning and decreases the response speed [9]. Research on transmission compliance and dynamic characteristics for precise control will be further required to overcome these issues.

In adapting the behavior of this compliant morphological type, the following essential assumptions need to be carefully considered for the tendon-driven mechanism:

(i) All under-tension tendons are used. The amount of stretch in tendons is proportionally small so that it can be neglected.
(ii) The connection of pulleys and tendons does not create sliding action.
(iii) The weight of the tendon is light so that it is possible to neglect the inertia, flexural bending, and shear effects of the tendon.
(iv) Each pulley must have a turning pair on its axis and a carrier(arm) between the pair of pulleys and tendons. This structure aims to keep the center distance of the corresponding pulleys stable.
(v) The manipulator configuration is typical of an articulated one, i.e., once the tendons and intermediate pulleys are removed, the manipulator transforms into an open-loop chain.

STRUCTURAL REPRESENTATIONS

For clarity and simplicity, we illustrate the conventional sketch of the TDM by highlighting only important functional elements in its kinematic configuration, such as shafts, pulleys, tendons, and links. It is also worth noting that one topological structure may result in a different design and representation for a planar configuration from a spatial one. Basically, in the TDM, there are two origin routing methods, namely the open-ended tendon and the endless tendon.

Functional Construction

In Figure 1 (*a*). a morphological of the open-ended tendon is demonstrated, in which one of the tendon's tips is attached to a movable-driven link. At the same time, another one is tied up to the driving pulley leading to the actuator. Along with the moving link to the actuator, there is a built-in transmission line in each tendon routing. Uniquely, the open-ended tendon embraces the unidirectional force, the force of friction, which transmits a real force but acts oppositely to the applied force to resist the body's motion [10]. In the first illustration shown in Figure 1 (*a*), the two corresponding pulleys, *i* and *j,* are connected by an open-ended tendon. The carrier/ link denoted by *k* is designed to keep a stable center range between the pulley, *i* and *j*.

Conversely, each belt or tendon in the endless type is spun among two corresponding pulleys with a stable center range in an endless chain. The driving pulley fixed on the rotating actuator can drive another pulley that is mechanically tied up to a control link. In another case, the driving pulley can be installed onto a pulley in the previous stage of the pulley train. It is shown in Fig. 2 (*b*) that the endless kinematic chain comprises the three stiff components, *i*, *j,* and *k,* and one compliant tendon. Another endless tendon feature is that it can be moved in either direction. The number of attached actuators, *m*, is generally the same as the number of degrees of freedom, *n* [11].

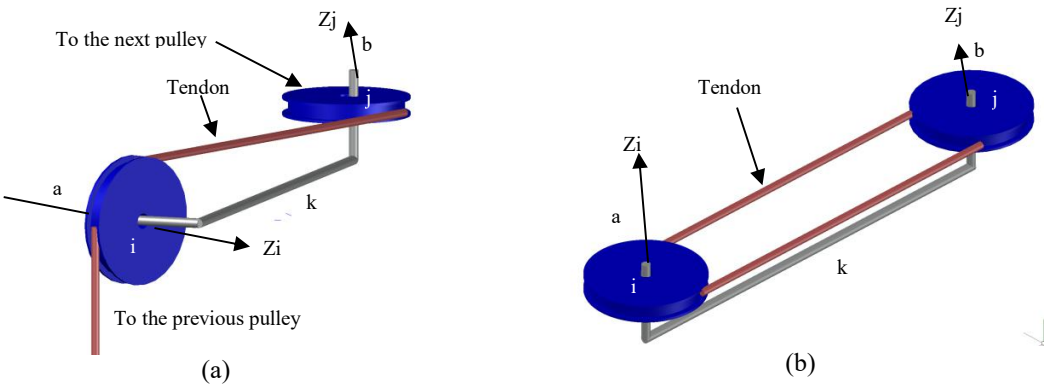

Figure 1. (a) Open-ended kinematic chain, (b) Endless kinematic chain

Planar Schematic Construction

In general, the routing method is classified into two types, namely the cross-type and the parallel-type. Figure 2 (*a*) demonstrates the cross kinematic chain when the belt or tendon route crosses to one and another pulley. In this case, the positive rotation generated by one pulley creates a negative value for another pulley. Contrarily, in Fig. 2(b), the belts or tendon spins simultaneously and rotates according to the previous pulley's orientation. In the parallel type, if one pulley rotates positively with respect to its carrier, it can also produce the same positive motion of the corresponding pulley.

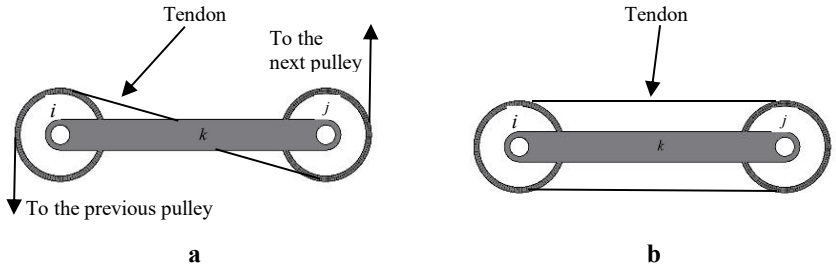

Figure 2. Two dimensional sketch illustrations of (a) open-ended (cross-type) and (b) endless (parallel) tendon [7]

Graph Construction

Once the tendon kinematic chain is defined, the joint connection between links is denoted by the edge connection between respective vertices to represent the graph theory. In addition, each pair of pulleys is wrapped up by a tendon routing and treated as a pulley pair. To distinguish different pair connections, we represent the turning pair by a thin-line edge, the parallel tendon routing type by a double-line edge, and the cross-tendon routing type by a bold edge. Additionally, the denoted thin edges are employed to locate their axis. Furthermore, this form of TDM graph is identical to the mechanism of the epicyclic gear train.

In implementing those rules, Table 1 shows the connections between Figure 3(*a*) and Figure 2(*a),* as well as Figure 3(*b*) and Figure 2(*b).*

Table 1 Graph Construction Comparison

Figure 3(a)	**Figure 2(a)**
Vertices *i*, *j* and *k*	Links *i*,*j*, and *k*
Thin edges *i*-*k* and *j*-*k*	Turning pairs that connect link *i* and *k*, and link *j* and *k*
Bold edge *i*-*j*	Cross-type routing that connect link *i* and *j*
Edge label *a* and *b*	Axis level *a* and *b*
Figure 3(b)	**Figure 2(b)**
Double-line edge	Parallel-type routing

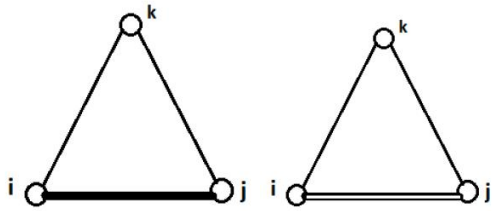

Figure 3 Graph representation (a). of Figure 2(a) and (b). of Figure 2(b)

STRUCTURAL CHARACTERISTICS

Similar to the epicyclic gear trains, the TDM graph can be identified by the following basic rules [8];

(i) In TDM, if a link is labeled as *n*, a degree-of-freedom is *F*, so the turning pair is (*n*-1), and the pulley pair is (*n*-*F*-1).

(ii) The whole of the double-line and bold edges need to be removed to make the subgraph become a tree. Exclusively, there is no circuit formed in thin edges.

(iii) Certain double-line or bold edge gained to the corresponding tree (subgraph) creates a fundamental circuit (*f*-circuit) that provides a double-line or bold edge and some thin edges.

(iv) The sum of the created double-line and bold edges are supposed to be the same as the number of *f*-circuits.

(v) The level of every thin edge corresponds to the axis position of a turning pair.

(vi) Every *f* -circuit has a transfer vertex that can distinguish the level of edges. The transfer vertex is assigned to the carrier/ link in a pulley train. If edges and the transfer vertex are on the same side, it has a similar level; Otherwise, if edges are on the contradictory side, it means the level is different.

MATHEMATICAL EQUATIONS

This section gives the f (fundamental) - circuit equation and coaxiality condition with respect to links, pulleys, and joint axis. A base pulley and the relationship of the joint angle is formulated by performing the relative rotation either in an open-loop or endless tendon configuration. Based on Tsai's model [8], the equations are detailed in the following;

Mathematical Equation of f-circuit

Initially, vertices underlie a pulley pair need to be assigned by *i* and *j*. This fundamental circuit scheme makes link *k* to be associated with the transfer vertex. The original form of tendon and pulley train is then created using links *i, j,* and *k*. Furthermore, with a pulley that rotates positively in every joint axis within the pulley pair, a fundamental (f-circuit) equation can be written as:

$$R_i\,\theta_{i,\,k} = \pm\, R_j\,\theta_{i,\,k} \tag{1}$$

where $\theta_{i,\,k}$ and $\theta_{j,\,k}$ represents the relative rotations of link *i* and *j* with respect to link *k,* respectively. R_i and R_j denote the radii of two assigned pulley, *i* and *j,* respectively.

It is also worth noting that the positive sign of Eq. (1) is associated with the parallel-type of tendon routing; either way, the cross-type is the negative one. The scheme of the parallel tendon with positive sign and cross tendon with a negative sign is also emphasized in [12], which the relative rotation in the Eq. (1) versus each joint axis of a pulley pair can be seen clearly in Fig. 4. In addition, Equation (1) is correct either the carrier is constantly tied up or not.

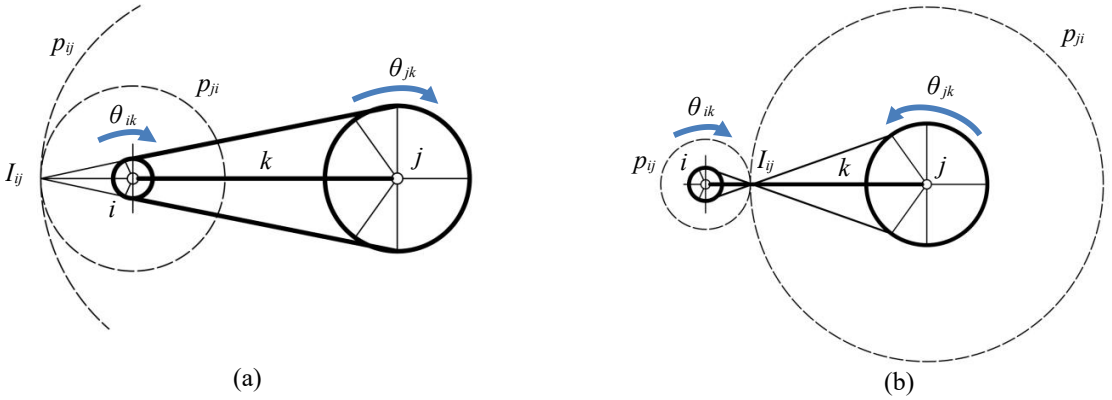

Figure 4 Relative Rotation of **(a)** parallel tendon with positive sign and **(b)** and cross tendon with negative sign

Coaxility Condition

As links *i, j,* and *k* employ a mutual joint axis, the condition is similar to the principle of the epicyclic gear trains. The equation relates to the relative rotations that can be used for three or more links sharing a common axis (coaxial), is given by:

$$\theta_{i,\,j} = \theta_{i,\,k} - \theta_{j,\,k} \tag{2}$$

Common Tendon-Driven Mechanism

In this section, Figure 4(a) will be elaborated with Eqs. (1) and (2) through the following process:

- Define the serial links that are linked by turning pairs. In this case, an open-loop chain formed comprise links 0, 1, 2, and 3.
- Define the consecutive joint axes, *a*, *b* and *c*.
- Classify the pulleys that are pivoted to the assigned joint axes, pulley *a*, *b* and *c* to the axes $j, j + 1, j + 2$.

- Categorize the pulleys that are free to rotate as j and $j + 1$ concerning link 0, 1, and 2.
- Define the tied rigid pulley that corresponds to link 3.
- Determine the base as link 0 and the link that is driven as link 3.
- Finally, figure out the rotation transformation occurring in the open-loop chain among the *base pulley j*, and all corresponding joint angles $\theta_{1,0}$, $\theta_{2,1,}$ and $\theta_{3,2.}$

Furthermore, Figure 5(b) is constructed to depict the figure 5(a) mechanism to obtain the corresponding graph representation. The graph in Fig. 5 (b) forms two units of f-circuits; (j, j + 1, 1) and (j + 1, 3, 2). The first two labels in the brackets represent the pulley pair's link numbers, while the rest is for the associated carrier. Then, the Eq. (1) is substituted for every *f*-circuits yield:

$$R_j \, \theta_{j,\,1} = R_{j+1} \, \theta_{j+1,\,1} \tag{3}$$

and

$$R_{j+1} \, \theta_{j+1,\,2} = R_{j+2} \, \theta_{3,\,2} \tag{4}$$

Because Link 0, 1, and j are coaxial, i.e., they share the same common joint axes, it can be written as

$$\theta_{j,\,1} = \theta_{j,\,0} - \theta_{1,\,0} \tag{5}$$

Likewise, link 1, 2, and $j + 1$ are coaxial too, so it can be written similarly as

$$\theta_{j+1,2} = \theta_{j+1,1} - \theta_{2,1} \tag{6}$$

By simultaneously substituting Eqs. (5) and (6) into (3) and (4), respectively, and then substituting $\theta_{j+1,1}$ from the two new equations, the following can be resulted;

$$\theta_{j,0} = \theta_{1,0} + (R_{j+1} / R_j) \, \theta_{2,1} + (R_{j+2} / R_j) \, \theta_{3,2} \tag{7}$$

In Eq. (7), the joint angles $\theta_{1,0,}$ $\theta_{2,1}$, $\theta_{3,2}$ influence the rotation of the base pulley, $\theta_{j,0.}$ Next, the equation associated with $(m + 1)$ links is given as follows

$$\theta_{j,0} = \theta_{1,0} \pm (R_{j+1} / R_j) \, \theta_{2,1} \pm (R_{j+2} / R_j) \, \theta_{3,2} \pm \ldots\ldots\ldots\ldots \pm (R_{j+m-1} / R_j) \, \theta_{m,\,m-1} \tag{8}$$

where the sign of every term $(R_{j+k-1} / R_j) \, \theta_{k,k-1,}$ refers to the number of cross-tendon routing type prior to the k_{th} joint axis. Furthermore, the even number of cross-type means positive sign; and vice versa. The Eq. (8) can be derived in order to get the partial rate of change of the base pulley rotation that correspond to the associated joint angle.

$$d\theta_{j,0} = d\theta_{1,0} \pm (R_{j+1} / R_j) \, d\theta_{2,1} \pm (R_{j+2} / R_j) \, d\theta_{3,2} \pm \ldots\ldots\ldots\ldots \pm (R_{j+m-1} / R_j) \, d\theta_{m,\,m-1} \tag{9}$$

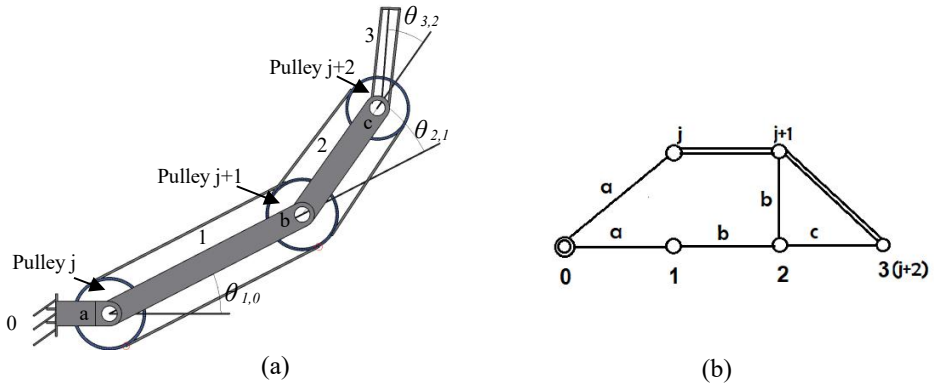

Figure 5 (a) Tendon-driven articulated mechanism and **(b)** Graph construction of Fig. 5(a)

While Figure 5 (a) illustrates the construction of the closed loop tendon, the open-loop tendon is shown in Fig. 6. The series connection of links 1, 2, and 3, the fixed frame denoted by 0, and the end-effector noted by pulley 4 shape the representation of the open-loop kinematic chain. In the figure below, Figliolini et al. [12] explained the construction of *n*-d.o.f.s mechanisms with an open-loop chain. The base pulley j can rotate to that of $j + 3$ by benefitting the angles $\theta_{1,0}$, $\theta_{2,1}$, $\theta_{3,2}$ and $\theta_{4,3.}$ The three circuits namely (j, j + 1, 1), (j + 1, j + 2, 2) and (j + 2, j + 3, 4) can represent the position equation. This circuit means that the first two terms in the parenthesis are the pulleys, while the last term shows the connecting link.

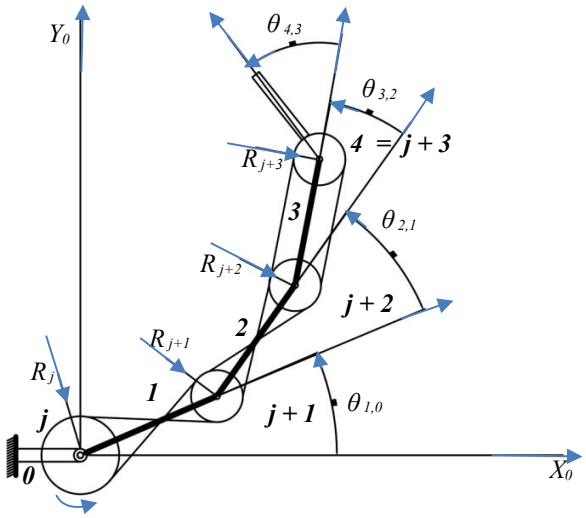

Figure 6 *n*-d.o.f.s articulated mechanism with open-loop chain

KINEMATICS SYNTHESIS OF TDM

In this section, a canonical graph as commonly used in bevel-gear trains is exploited to investigate the topological structure and analyze the TDM kinematics in an open-loop routing [8]. Firstly, the relation of the position, orientation, and the joint angles of the end-effector is characterized with the equivalent open-loop routing. Next, the joint angles are linked to the rotational transformation of the base pulleys. In the following, one Case Study is investigated to demonstrate the principles before the proposed design is presented.

Case Study: The Endless Routing of Three-DOF Robotic Manipulator

In Figure 7, the two-dimensional sketch drawing of a three DOF manipulator arm is shown. It has the following main features:

- Pulleys that are free to rotate: 4 and 5 correspond to the axis *a*, axis *b* correspond with pulleys 2 and 6, and pulley 3 correspond to axis *c*.
- Driving link that acts as a carrier: the 1st driving link corresponds to both pulley pairs (4,2) and (5,6), the 2nd rigid link for pulley pairs (6,3), and the 3rd moving link for pulley 3.
- Tendon connection for the pulley: the 1st corresponds to pulley 4 and 2, and the 2nd refers to pulley 5, 6 and 3.

Figure 8(*a*) demonstrates the canonical graph of the associated three DOF schematic mechanisms. Figure 6(b) illustrates the transmission line of the two tendons corresponding to the equivalent open-loop chain

- links connected in series in an open-loop chain: links 0, 1, 2, and 3.
- Fundamental circuits: (2, 4, 1), (5, 6, 1) and (3, 6, 2).
- The double line represents the parallel-type routing of the mechanism.

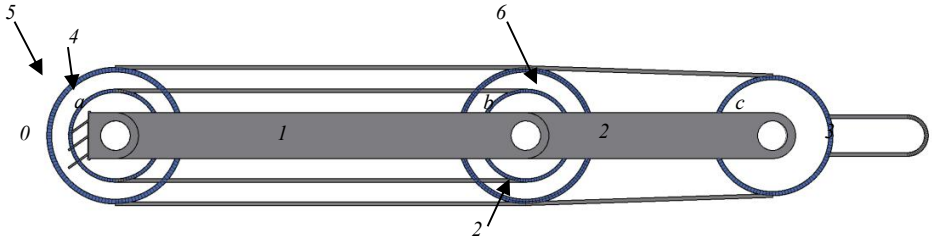

Figure 7. Two-dimensional sketch drawing of a three DOF robotic manipulator

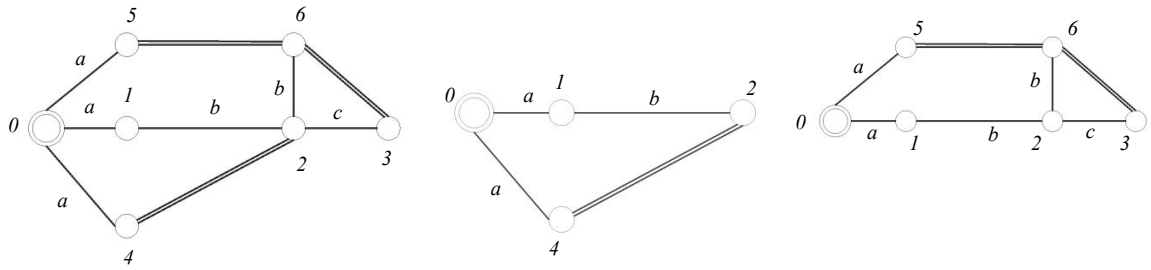

(a) (b)

Figure 8 (a) Canonical graph of Fig. 8(a) and **(b)** Two tendon drives

Eq. (8) then can be substituted into the two tendon routings as follows:

$$\theta_{4,0} = \theta_{1,0} + (R_2 / R_4)\,\theta_{2,1} \tag{10}$$

and

$$\theta_{5,0} = \theta_{1,0} + (R_6 / R_5)\,\theta_{2,1} + (R_3 / R_5)\,\theta_{3,2} \tag{11}$$

where R_j, $j = 2, 3, 4, \ldots$ denotes the radii of the pulley in Fig. 6(*a*). Next, the identity equation $\theta_{1,0} = \theta_{1,0}$ is added to Eqs. (10) and (11) respectively, and form to a matrix as follows

$$\begin{bmatrix} \theta_{1,0} \\ \theta_{4,0} \\ \theta_{5,0} \end{bmatrix} = \begin{bmatrix} 1 & 0 & 0 \\ 1 & R2/R4 & 0 \\ 1 & R6/R5 & R3/R5 \end{bmatrix} \begin{bmatrix} \theta_{1,0} \\ \theta_{2,1} \\ \theta_{3,2} \end{bmatrix} \tag{12}$$

Eq. (12) gives the important transformation between the angular displacements of the input links ($\theta_{1,0}$, $\theta_{4,0}$, and $\theta_{5,0}$) and the joint angles ($\theta_{1,0}$, $\theta_{2,1}$, and $\theta_{3,2}$). The resulted transformations are linear and can be inversely transformed into the matrix below. As a dummy step, $R_4 = R_2$ and $R_5 = R_6 = R_3$, Eq. (12) can be turned into the following

$$\begin{bmatrix} \theta_{1,0} \\ \theta_{4,0} \\ \theta_{5,0} \end{bmatrix} = \begin{bmatrix} 1 & 0 & 0 \\ 1 & 1 & 0 \\ 1 & 1 & 1 \end{bmatrix} \begin{bmatrix} \theta_{1,0} \\ \theta_{2,1} \\ \theta_{3,2} \end{bmatrix} \tag{13}$$

and the inverse matrix becomes;

$$\begin{bmatrix} \theta_{1,0} \\ \theta_{2,1} \\ \theta_{3,2} \end{bmatrix} = \begin{bmatrix} 1 & 0 & 0 \\ -1 & 1 & 0 \\ 1 & -1 & 1 \end{bmatrix} \begin{bmatrix} \theta_{1,0} \\ \theta_{4,0} \\ \theta_{5,0} \end{bmatrix} \tag{14}$$

It is noted that the second and the third joint cannot move when links 1 and 4 are driven at the same rate, and both the joints are tied if links 1, 4, and 5 are placed at the same state.

Proposed design: Open Hand Yale Model T (Two DOF Robotic Gripper)

The proposed design utilizes past work from Open Hand Yale Model T. Each underactuated hand has two-link fingers coupled with finger pads and a rubber-flexure joint. The flexure joints were fabricated by PMC-780 rubber urethane, and the finger pads were made with Vytaflex 40 urethane [13].

Figure 9(*a*) illustrates the planar schematic drawing of a two DOF gripper.

- Pulleys that are free to rotate: pulley 3 with respect to axis *a*, and 4 with respect to axis *b*
- The moving link acts as a carrier: the 1st moving link for pulley pairs (3,4) and the 2nd rigid link attached for pulley 4.
- The actuators are attached to the fixed frame of the robot arm, denoted by series of slashes before the 1st moving link (0).
- Link 2 is remotely driven by means of an endless kinematic chain through pulleys 4 and 3.

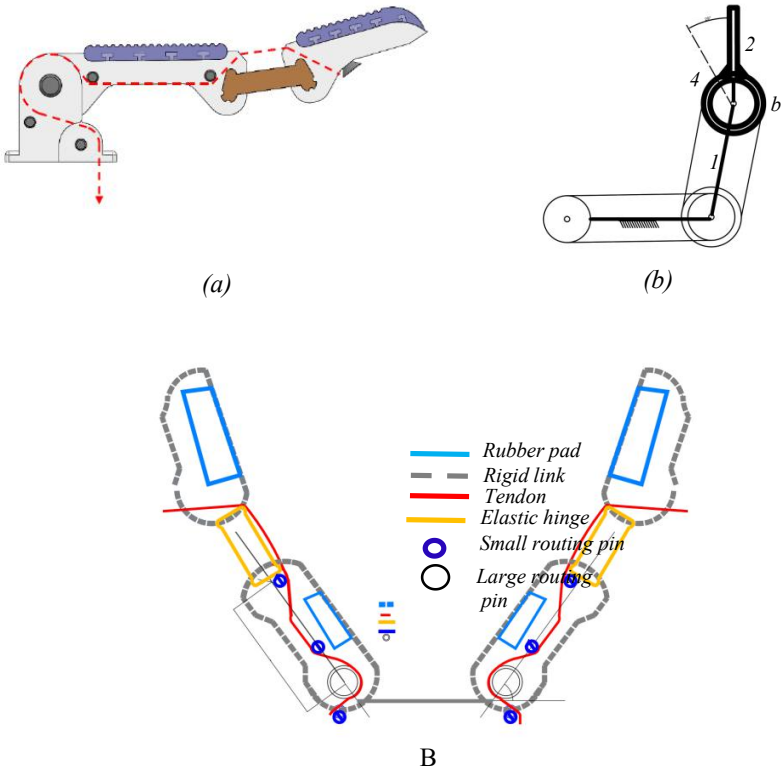

Figure 9 (*a*) Schematic of Openhand Yale Model T and (b) Canonical Graph of Fig. 9(*a*)

CONCLUSIONS

In this paper, a systematic review of some recent technological advances in soft robotic grippers has been presented. The approach for designing a soft gripper was by combining rigid links with tendon and soft elastomer. The chosen model was the openhand Yale model T which employs soft rubber to connect to each rigid link. Our study made the simplified model of kinematic analysis of Tendon driven mechanism based on a canonical used in bevel-gear trains. It was exploited to investigate the topological structure and analyze the kinematic of TDM in an open-loop chain [8]. Firstly, the relation of the position, orientation, and the joint angles of the end-effector was characterized with the equivalent open-loop chain. Then, the joint angles linked to the rotational transformation of the base pulleys were analyzed in great detail. The kinematic analysis of the proposed design of openhand Yale model T was made.

The future work includes, but is not limited to, the detailed design and development of the proposed design on the soft robotic hand based on the abovementioned openhand Yale model T, prototyping and testing on real-world applications to handle delicate objects and adjust to unstructured and asymmetric shapes, etc.

ACKNOWLEDGMENTS

The authors would like to thank the Department of Design, Manufacturing, and Engineering Management (DMEM), University of Strathclyde, for its kind support in conducting this investigation into the soft robotics - project in mechatronics and automation from the Robotics and Autonomous Systems (RAS) Group.

REFERENCES

1. J. Fraś, M. Maciaś, F. Czubaczyński, P. Salek, and J. Glówka, “Soft flexible gripper design, characterization and application,” *Adv. Intell. Syst. Comput.*, vol. 543, no. December 2016, pp. 368–377, 2017, doi: 10.1007/978-3-319-48923-0_40.
2. F. Connolly, C. J. Walsh, and K. Bertoldi, “Automatic design of fiber-reinforced soft actuators for trajectory matching,” *Proc. Natl. Acad. Sci. U. S. A.*, vol. 114, no. 1, pp. 51–56, 2017, doi: 10.1073/pnas.1615140114.
3. J. Shintake, V. Cacucciolo, D. Floreano, and H. Shea, “Soft Robotic Grippers,” *Adv. Mater.*, vol. 30, no. 29, 2018, doi: 10.1002/adma.201707035.
4. M. Manti, T. Hassan, G. Passetti, N. D’Elia, C. Laschi, and M. Cianchetti, “A Bioinspired Soft Robotic Gripper for Adaptable and Effective Grasping,” *Soft Robot.*, vol. 2, no. 3, pp. 107–116, 2015, doi: 10.1089/soro.2015.0009.
5. A. McLaren, Z. Fitzgerald, G. Gao, and M. Liarokapis, “A Passive Closing, Tendon Driven, Adaptive Robot Hand for Ultra-Fast, Aerial Grasping and Perching,” *IEEE Int. Conf. Intell. Robot. Syst.*, no. August, pp. 5602–5607, 2019, doi: 10.1109/IROS40897.2019.8968076.
6. A. Bicchi, “Hands for dexterous manipulation and robust grasping: A difficult road toward simplicity,” *IEEE Trans. Robot. Autom.*, vol. 16, no. 6, pp. 652–662, 2000, doi: 10.1109/70.897777.
7. M. Uyguroğlu and H. Demirel, “Kinematic analysis of tendon-driven robotic mechanisms using oriented graphs,” *Acta Mech.*, vol. 182, no. 3–4, pp. 265–277, 2006, doi: 10.1007/s00707-005-0298-z.
8. L. W. Tsai and J. J. Lee, “Kinematic analysis of tendon-driven robotic mechanisms using graph theory,” *J. Mech. Des. Trans. ASME*, vol. 111, no. 1, pp. 59–65, 1989, doi: 10.1115/1.3258972.
9. S. L. Chang, J. J. Lee, and H. C. Yen, “Kinematic and compliance analysis for tendon-driven robotic mechanisms with flexible tendons,” *Mech. Mach. Theory*, vol. 40, no. 6, pp. 728–739, 2005, doi: 10.1016/j.mechmachtheory.2004.11.003.
10. Y. H. Lee and J. J. Lee, “Modeling of the dynamics of tendon-driven robotic mechanisms with flexible tendons,” *Mech. Mach. Theory*, vol. 38, no. 12, pp. 1431–1447, 2003, doi: 10.1016/S0094-114X(03)00096-X.
11. L. Tsai, “Design of Tendon-Driven Manipulators,” vol. 117, no. June 1995, 2016.
12. G. Figliolini, C. Lanni, L. Di Donato, R. Melloni, and A. P. Bacchetta, *Kinematic Synthesis of a Tendon-Driven Robotic Arm*, vol. 91, no. November 2020. Springer International Publishing, 2021.
13. R. R. Ma and A. M. Dollar, “An underactuated hand for efficient finger-gaiting-based dexterous manipulation,” *2014 IEEE Int. Conf. Robot. Biomimetics, IEEE ROBIO 2014*, pp. 2214–2219, 2014, doi: 10.1109/ROBIO.2014.7090666.